



The SH3 domain of Fyn kinase interacts with and induces liquid–liquid phase separation of the low-complexity domain of hnRNPA2

Received for publication, July 30, 2018, and in revised form, October 27, 2018 Published, Papers in Press, November 5, 2018, DOI 10.1074/jbc.RA118.005120

Joshua Amaya^{†1,2}, Veronica H. Ryan^{§1,3}, and Nicolas L. Fawzi^{†‡4}

From the [†]Department of Molecular Pharmacology, Physiology, and Biotechnology and the [§]Graduate Program in Neuroscience, Brown University, Providence, Rhode Island 02912

Edited by Norma M. Allewell

Liquid–liquid phase separation of proteins and nucleic acids into membraneless organelles (MLOs) spatially organizes cellular components and reactions. The RNA-binding protein heterogeneous nuclear ribonucleoprotein A2 (hnRNPA2) carries mRNA targets in MLOs called transport granules in neurons and oligodendrocytes. At sites of local translation, hnRNPA2 is phosphorylated by the tyrosine protein kinase Fyn, releasing the mRNA for translation. Fyn recognizes targets through its SH3 domain (Fyn-SH3). However, hnRNPA2 lacks canonical SH3-binding sequences, raising the question of how Fyn-SH3 binds hnRNPA2 in phase-separated transport granules. Here, we characterize the structural details of the interaction of the hnRNPA2 low-complexity domain (LC) with Fyn-SH3 and the effect of Fyn-SH3 on hnRNPA2 phase separation. We combined *in vitro* microscopy and solution NMR spectroscopy to evaluate assembly of hnRNPA2 and Fyn-SH3 into *in vitro* phase-separated granules and probe the structural details of their interaction. We observed that Fyn-SH3 induces hnRNPA2 LC phase separation and that Fyn-SH3 is incorporated into *in vitro* hnRNPA2 LC granules. Moreover, we identified hnRNPA2 LC interaction sites on the surface of Fyn-SH3. Our data offer a structural view of how hnRNPA2 LC may interact with Fyn. To our knowledge, our study provides the first example of a single globular domain inducing phase separation of a disordered MLO scaffold protein.

Liquid–liquid phase separation (LLPS)⁵ is a proposed mechanism for the formation of membraneless organelles (MLOs) (1–3). LLPS of MLOs can serve to spatially organize cellular components and has been proposed to speed enzymatic reactions as a result of concentrating reactants (4) or by providing a unique chemical environment (5–7). LLPS is an equilibrium process where molecules assemble into two or more distinct phases that differ in concentrations and potentially in structures and contacts (6). Disparate MLOs from nucleoli and nuclear speckles to stress granules and processing bodies carry out different cellular functions and are composed of a variety of cellular components (8, 9). RNA granules represent a class of MLOs that are enriched in RNA and RNA-binding proteins. Here we focus on RNA transport granules containing the heterogeneous nuclear ribonucleoprotein hnRNPA2 (10).

hnRNPA2 is an RNA-binding protein involved in pre-mRNA splicing, translation control, and mRNA transport (10). The domain structure of hnRNPA2 includes two N-terminal RNA recognition motifs that together bind a consensus RNA sequence known as the A2 response element (11), followed by an intrinsically disordered domain of low amino acid sequence complexity (low-complexity domain (LC)) (12). This LC has a subregion that is classified as a prion-like domain with amino acid sequence composition resembling aggregation-prone yeast prions (*i.e.* enriched in glutamine, asparagine, serine, and tyrosine) (13). Many prion-like domain-containing proteins including hnRNPA2 have been implicated in the formation of cellular inclusions seen in neurodegenerative diseases (14, 15). Importantly, the LC of hnRNPA2 is necessary and sufficient for LLPS and aggregation (12). In its physiological role in the nervous system, hnRNPA2 forms mRNA transport granules to bring mRNAs, including myelin basic protein mRNA and activity regulated cytoskeleton-associated protein (Arc) mRNA, to sites of local translation in dendrites and oligodendroglial processes (16). When the granule reaches sites of local translation, the Src-family tyrosine kinase Fyn phosphorylates hnRNPA2, which releases cargo mRNA molecules for translation (17).

This work was supported in part by NIGMS, National Institutes of Health, Grants R01GM118530 (to N. L. F.) and P20GM104937. The authors declare that they have no conflicts of interest with the contents of this article. The content is solely the responsibility of the authors and does not necessarily represent the official views of the National Institutes of Health.

This article was selected as one of our Editors' Picks.

This article contains Figs. S1–S3.

The NMR spectroscopy data reported in this paper have been submitted to the Biological Magnetic Resonance Data Bank (BMRB) under BMRB accession number 27649.

¹ Both authors contributed equally to this work.

² Supported in part by two summer Karen T. Romer Undergraduate Teaching and Research Awards.

³ Supported in part by T32MH020068, a Graduate Award from the Robert J. and Nancy D. Carney Institute for Brain Science at Brown University, and NINDS, National Institutes of Health, Grant F31NS110301.

⁴ To whom correspondence should be addressed: Dept. of Molecular Pharmacology, Physiology, and Biotechnology, Brown University, Providence, RI 02912. Tel.: 401-863-5232; Fax: 401-863-6087; E-mail: nicolas_fawzi@brown.edu.

⁵ The abbreviations used are: LLPS, liquid–liquid phase separation; hnRNPA2, heterogeneous nuclear ribonucleoprotein A2; MLO, membraneless organelle; LC, low-complexity domain; SH2 and SH3, Src homology 2 and 3, respectively; HSQC, heteronuclear single quantum correlation; DIC, differential interference contrast; BisTris, 2-[bis(2-hydroxyethyl)amino]-2-(hydroxymethyl)propane-1,3-diol; NLS, nuclear localization signal; TEV, tobacco etch virus.

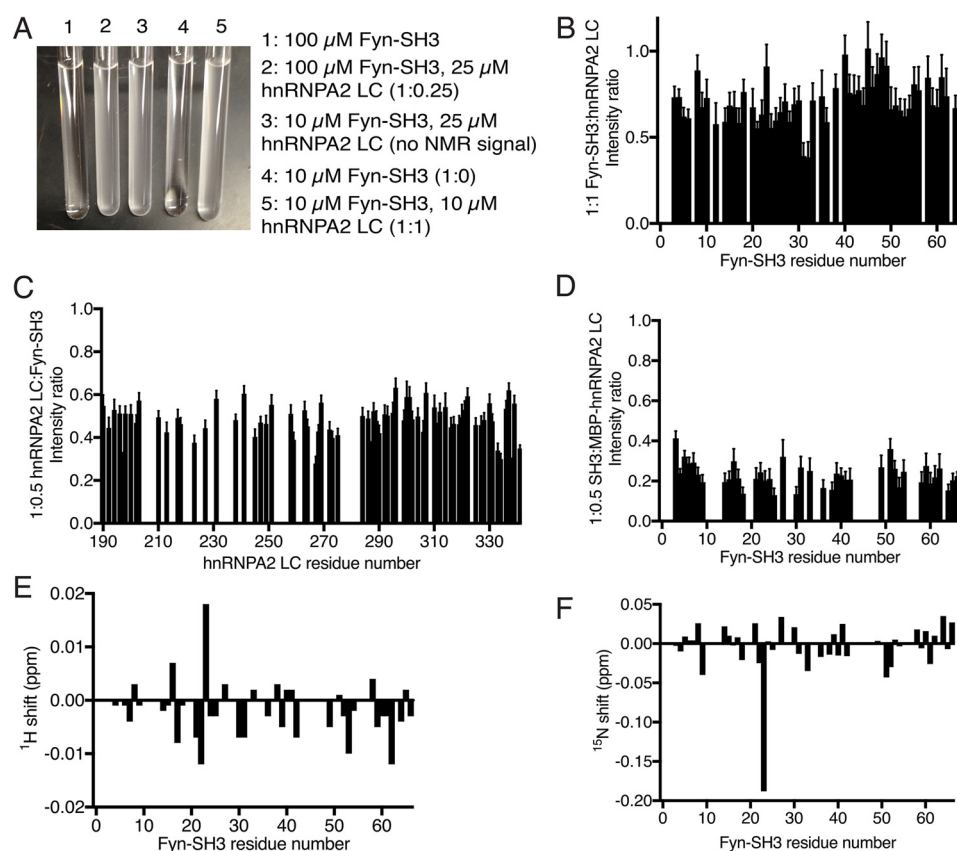


Figure 1. LLPS is observed when Fyn-SH3 is added to hnRNP A2 LC in both untagged and solubility-tagged forms. A, observations of turbidity at different titrations of [^{15}N]Fyn-SH3 to hnRNP A2 LC WT in NMR tubes. B, intensity ratios for 1:1 [^{15}N]Fyn-SH3 (10 μM) to hnRNP A2 LC WT (10 μM) compared with [^{15}N]Fyn-SH3 (10 μM) alone. C, intensity ratios for the 1:0.5 [^{15}N]hnRNP A2 LC WT (20 μM) to unlabeled Fyn-SH3 at different amino acid residues. Buffer conditions: 20 mM MES, pH 5.5. D, the addition of MBP-tagged hnRNP A2 LC to Fyn-SH3 at a ratio of 1:0.5 resulted in decreased signal intensity. At higher concentrations of MBP-hnRNP A2 LC, no signal from [^{15}N]Fyn-SH3 is observed. Buffer conditions: 20 mM NaP_i, pH 6.1, 50 mM NaCl. E and F, ^1H (E) and ^{15}N (F) chemical shift perturbations for 1:0.5 [^{15}N]Fyn-SH3 to solubility-tagged MBP-hnRNP A2 LC WT are small because the interacting Fyn-SH3 is effectively NMR-invisible when partitioned into LLPS droplets. Buffer conditions: 20 mM NaP_i, pH 6.1, 50 mM NaCl.

Fyn kinase is composed of several different Src homology domains in addition to the catalytic domain (16). The SH3 domain mediates protein–protein interactions with target proteins and putatively binds peptides containing a PXXP motif (18), whereas the SH2 domain binds primarily to phosphorylated tyrosines. Initially, Fyn is in a closed conformation, but when it is phosphorylated and activated, the protein adopts an open conformation, making the SH2 and SH3 available to downstream targets (19). Fyn activation triggers phosphorylation of hnRNP A2 and other granule components, including hnRNPF, resulting in the dissociation of the granule and removal of translational repression (17). Whereas the functional interaction between hnRNP A2 and Fyn is well-understood, the physical interaction between Fyn kinase and hnRNP A2 is still unclear. Indeed, hnRNP A2 lacks a PXXP motif, the canonical SH3-binding motif. Therefore, a clearer picture of the structural details and interaction between hnRNP A2 LC and the SH3 domain of Fyn kinase is necessary. We hypothesized that the SH3 domain of Fyn interacts with disperse and phase-separated forms of hnRNP A2 LC. Here, we used NMR spectroscopy and microscopy to probe hnRNP A2–Fyn-SH3 protein–protein interactions and the effect of hnRNP A2 disease-associated mutations on their interaction and hnRNP A2 assembly.

Results

Fyn-SH3 interacts with hnRNP A2 LC

We performed titration experiments using NMR to determine which regions of hnRNP A2 LC mediate interactions with Fyn-SH3. Initially, we attempted to quantify the effect of the addition of unlabeled (NMR-silent) hnRNP A2 LC WT on the two-dimensional “fingerprint” ^1H - ^{15}N NMR correlation (HSQC) spectrum of Fyn-SH3 incorporating ^{15}N stable isotope. However, the addition of 0.25 molar eq of natural isotopic abundance (*i.e.* NMR-silent) hnRNP A2 LC (1:0.25 [^{15}N]Fyn-SH3 to hnRNP A2 LC; *i.e.* 100 μM Fyn and 25 μM hnRNP A2 LC) led to sample opalescence consistent with LLPS (Fig. 1A). Further increase in hnRNP A2 LC concentration decreased the NMR intensity significantly (Fig. 1B), and NMR signal was lost entirely with 1:2.5 ^{15}N -labeled Fyn-SH3 to hnRNP A2 LC. Correspondingly, when we titrated ^{15}N -labeled hnRNP A2 LC WT with natural abundance Fyn-SH3, we saw a decrease in intensity at 1:0.5 hnRNP A2 LC–Fyn-SH3 (Fig. 1C), and signal was lost entirely in at 1:1. Importantly, hnRNP A2 LC alone does not phase-separate at these solution conditions (in the absence of salt) (12); therefore, these data suggest that Fyn-SH3 induces phase separation of hnRNP A2 LC. In an attempt to reduce phase separation of hnRNP A2 LC/Fyn-SH3 to reveal

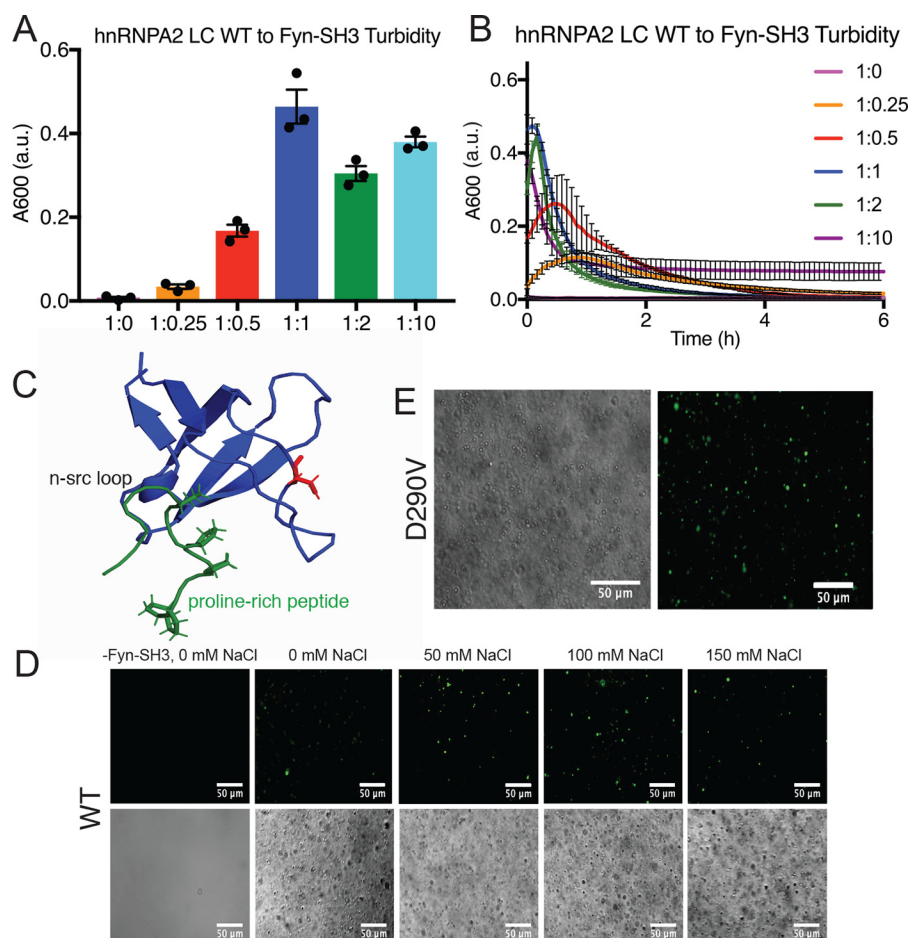


Figure 2. Fyn-SH3 induces hnRNP A2 LC phase separation and is incorporated into hnRNP A2 LC droplets. *A*, A_{600} (arbitrary units (a.u.)) measurements of 20 μ M hnRNP A2 LC WT at increasing concentrations of Fyn-SH3. *B*, an increase in concentration of Fyn-SH3 in the presence of 20 μ M hnRNP A2 LC WT leads to an increase in hnRNP A2 LC WT turbidity until turbidity returns to baseline at later time points for all but the highest excess of Fyn-SH3. *C*, structural model of Fyn-SH3 bound to a proline-rich protein from Protein Data Bank entry 1A0N showing where the Alexa Fluor label was placed in this study (red). *D* (top), fluorescence microscopy of 1:0.5 hnRNP A2 LC WT to Alexa Fluor-labeled Fyn-SH3 at increasing salt concentrations shows that Fyn-SH3 enters hnRNP A2 LC droplets. Bottom, DIC microscopy of 1:0.5 hnRNP A2 LC WT to Alexa Fluor-labeled Fyn-SH3 at increasing salt concentrations. The first column (top and bottom) represents the control (1:0.001 hnRNP A2 LC to Alexa Fluor-labeled Fyn-SH3) with 0 mM NaCl. *E*, DIC and fluorescence microscopy of 1:0.5 hnRNP A2 LC D290V to Alexa Fluor-labeled Fyn-SH3. Buffer was 20 mM MES, pH 5.5. Scale bar, 50 μ m.

the specific binding sites on Fyn-SH3, we used a highly soluble form of hnRNP A2 LC with an N-terminal maltose-binding protein solubility tag, MBP-hnRNP A2 LC (12). This tagged form of hnRNP A2 LC does not phase-separate in buffers with conductivities in the physiological range (here, we use 20 mM NaP_i, 50 mM NaCl, pH 6.1). Surprisingly, we still observed a loss of signal intensity upon mixing the peptides at a ratio of 1:0.5 [¹⁵N]Fyn-SH3 to MBP-hnRNP A2 LC, indicative of the formation of a large, NMR-invisible species, and the solution turned cloudy (Fig. 1D). Quantification at ratios beyond 1:0.5 was impossible as no Fyn-SH3 signal remained (consistent with Fyn-SH3 partitioning into the protein-dense phase), and chemical shifts were small at 1:0.5 (Fig. 1, E and F). Significantly, these experiments with tagged hnRNP A2 LC were done in 50 mM NaCl, indicating that the interaction between monomeric Fyn-SH3 and monomeric hnRNP A2 LC is not dependent on weak electrostatic interactions artificially increased in the 0 mM salt conditions used for untagged hnRNP A2 LC. Therefore, Fyn-SH3 robustly induces phase separation of hnRNP A2 LC. As such, we decided to investigate the effect of Fyn-SH3 on hnRNP A2 LC phase separation further.

Fyn-SH3 increases the turbidity of hnRNP A2 LC WT

Our observation of reduced NMR signal intensity and enhanced optical turbidity for ¹⁵N-labeled hnRNP A2 LC to Fyn-SH3 titrations upon mixing intrigued us. To quantify phase separation of hnRNP A2 LC as a function of Fyn-SH3 concentration, we measured sample turbidity (Fig. 2A). As the concentration of Fyn-SH3 increases, the turbidity of hnRNP A2 LC WT increases up to equimolar concentrations of Fyn-SH3. In addition, we measured the turbidity over the course of 6 h (Fig. 2B). The turbidity increased for each titration over a short time, consistent with sample mixing, and then decreased until the turbidity reached baseline levels, consistent with droplet coarsening to larger sizes than the wavelength of light and droplet sedimentation and adherence to walls of the well. At 1:1 and 1:2, similar time courses and maximum turbidity values are observed. At 1:10 only, turbidity does not return to baseline by the 6-h time point (Fig. 2B).

To analyze the effects of the disease mutations of hnRNP A2 on the interaction with Fyn-SH3, we performed turbidity experiments with hnRNP A2 LC disease mutants (D290V or

P298L) with increasing concentrations of Fyn-SH3. As the concentration of Fyn-SH3 increases, the turbidity of both D290V and P298L samples increase (Fig. S1, A and B). These results were similar to the results obtained in the hnRNPA2 LC WT experiment (Fig. 2A).

Fyn-SH3 incorporates into hnRNPA2 LC droplets

As loss of NMR signal and turbidity could arise from aggregation or LLPS, we used differential interference contrast (DIC) microscopy to show that the turbidity observed for Fyn-SH3 and hnRNPA2 LC samples arises from LLPS. Furthermore, we did this experiment along with fluorescence microscopy to better understand the role that Fyn-SH3 plays in LLPS. To test the hypothesis that Fyn-SH3 co-phase separates with hnRNPA2 LC, we placed an Alexa Fluor label on Fyn-SH3 away from the proline binding site that was identified previously (20) (Fig. 2C) by mutating a surface-exposed serine residue (Ser-25) to cysteine. In 0 mM NaCl buffer, DIC microscopy images show that the addition of Fyn-SH3 induces the formation of hnRNPA2 LC WT liquid droplets at a concentration and solution conditions where hnRNPA2 LC alone does not phase-separate (Fig. 2D, second column, bottom panel) (12). Additionally, fluorescence microscopy data demonstrate that Fyn-SH3 incorporates into the droplets (Fig. 2D, second column, top panel). Furthermore, Fyn-SH3 induces droplet formation of the hnRNPA2 LC D290V mutant (Fig. 2E).

Now that we could conclude that Fyn-SH3 induces hnRNPA2 LC phase separation at 0 mM NaCl, we performed experiments at increasing salt concentrations to determine whether Fyn-SH3 is incorporated into LLPS droplets of hnRNPA2 LC at physiological salt conditions. Regardless of the concentration of NaCl, incorporation of Fyn-SH3 in the hnRNPA2 LC WT droplets was still observed, and the morphology of the droplets did not change (Fig. 2D). These results demonstrate that the interaction between Fyn-SH3 and hnRNPA2 LC is not an artifact of the low-salt conditions used for NMR experiments.

Fyn-SH3 may reduce the aggregation of hnRNPA2 disease-associated mutants

We previously showed that hnRNPA2 mutants D290V and P298L lead to conversion of liquid, phase-separated hnRNPA2 LC droplets to protein aggregates (12). To determine whether Fyn-SH3 binding can disrupt or encourage conversion of hnRNPA2 from a liquid form to an aggregated form associated with disease, we incubated hnRNPA2 LC and its disease-associated variants D290V and P298L with and without Fyn-SH3. We mixed Fyn-SH3 with hnRNPA2 LC WT, D290V, or P298L and then visualized the morphology of the phase-separated assemblies using DIC microscopy at two time points (0 and 3 h). The addition of Fyn-SH3 to hnRNPA2 LC WT did not change the morphology of the droplets as the droplets predominantly maintained a round shape (Fig. 3A, top). In comparison, after 3 h, the hnRNPA2 LC disease mutant proteins in the absence of Fyn-SH3 appear irregularly shaped, consistent with the formation of irreversible aggregation (12, 21) (Fig. 3A, middle and bottom). Aggregation was most prominent in the P298L disease mutant (Fig. 3A, bottom). When Fyn-SH3 was added to the

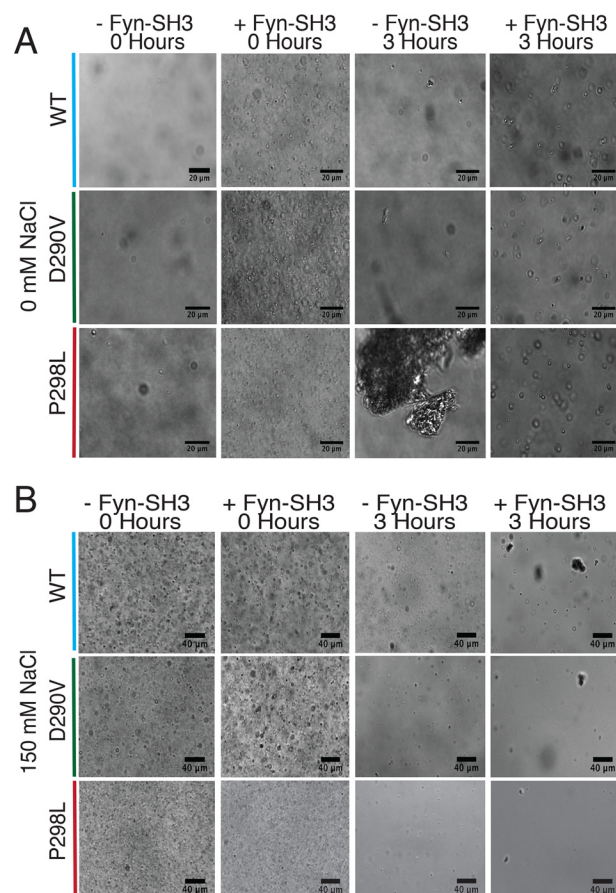


Figure 3. Fyn-SH3 delays formation of aggregates of hnRNPA2 P298L disease mutants. A, DIC microscopy of hnRNPA2 LC WT with or without Fyn-SH3 at 0 and 3 h (top), hnRNPA2 LC D290V with or without Fyn-SH3 at 0 and 3 h (middle), and hnRNPA2 LC P298L with or without Fyn-SH3 at 0 and 3 h (bottom) in the presence of 0 mM NaCl. Scale bar, 20 μm. B, DIC microscopy of hnRNPA2 LC WT with or without Fyn-SH3 at 0 and 3 h (top), hnRNPA2 LC D290V with or without Fyn-SH3 at 0 and 3 h (middle), and hnRNPA2 LC P298L with or without Fyn-SH3 at 0 and 3 h (bottom) in the presence of 150 mM NaCl. Scale bar, 40 μm. Buffer was 20 mM MES, pH 5.5.

hnRNPA2 LC P298L mutant, after 3 h, aggregation into irregular structures was not apparent, and round droplets were present instead (Fig. 3A, bottom). For the D290V mutant, both aggregation and droplets are observed, suggesting that the effect is not as prominent as for the P298L mutant (Fig. 3A, middle). These results suggest that Fyn-SH3 delays hnRNPA2 LC P298L aggregation. We repeated this same experiment at the same conditions but with different protein stocks and observed the same change in P298L aggregation (Fig. S2A). Furthermore, Fyn-SH3 still incorporates into hnRNPA2 LC P298L droplets despite the propensity to aggregate over time (Fig. S2B). Unfortunately, we were not able to quantify the effect by other approaches; turbidity is enhanced by both LLPS and aggregation, and amyloid-labeling dyes also fluoresce in liquid droplets (22). To test the effects of salt on the aggregation of hnRNPA2 disease mutants, we ran similar experiments to the DIC microscopy experiments in Fig. 2A but used buffer with physiological 150 mM NaCl in place of 0 mM NaCl. Unlike at low salt, hnRNPA2 LC aggregation still occurs at 150 mM NaCl even in the presence of Fyn-SH3 (Fig. 3B). After 3 h, the WT, D290V, and P298L samples were still aggregated, with or without Fyn-

Fyn-SH3 induces hnRNP A2 LC phase separation

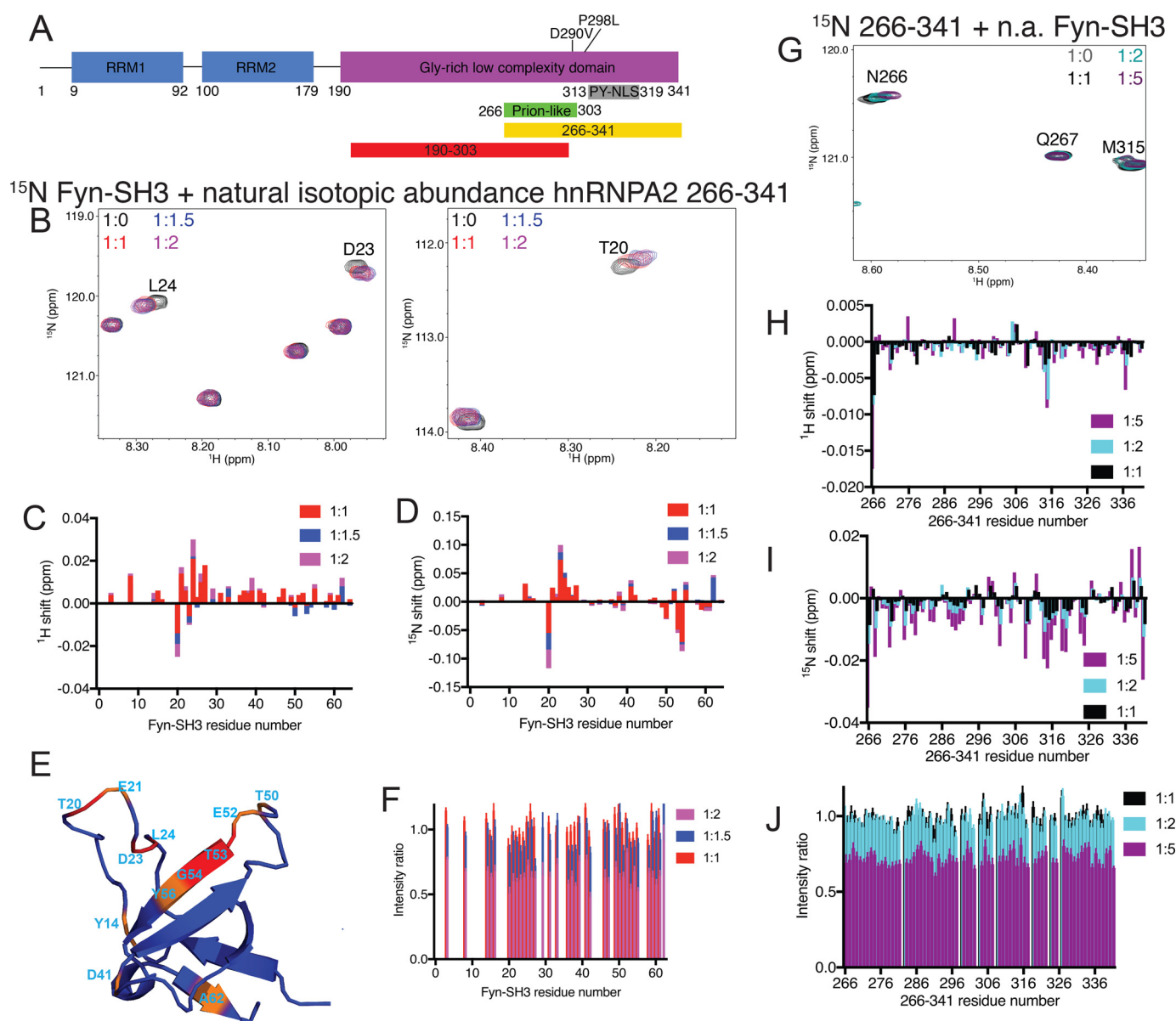


Figure 4. hnRNP A2 LC subpeptide gives insight into Fyn-SH3 binding sites. *A*, domain structure of hnRNP A2. *B*, examples of shifting peaks in ^1H ^{15}N HSQC of $20\ \mu\text{M}$ ^{15}N Fyn-SH3 titrated with increasing amounts of hnRNP A2 266–341: 1:0 (black), 1:1 (red), 1:1.5 (blue), and 1:2 (magenta) ^{15}N Fyn-SH3 to hnRNP A2 266–341 titrations. *C* and *D*, ^1H (*C*) and ^{15}N (*D*) chemical shift perturbations seen in ^{15}N Fyn-SH3 to hnRNP A2 266–341 titrations. *E*, heat map of Fyn-SH3 showing residues with ^{15}N chemical shift perturbations greater than 0.02 ppm (orange) and greater than 0.05 ppm (red). The Fyn-SH3 structure is from Protein Data Bank entry 1A0N. *F*, intensity ratio for the ^{15}N Fyn-SH3 to hnRNP A2 266–341 titration. Buffer was 20 mM MES, pH 5.5. *G*, ^1H ^{15}N HSQC of the peaks with large chemical shifts in the ^{15}N hnRNP A2 266–341 to Fyn-SH3 titration. *H* and *I*, ^1H (*H*) and ^{15}N (*I*) chemical shift perturbations of ^{15}N hnRNP A2 266–341 to Fyn-SH3 show the largest ^{15}N chemical shift perturbations in the region around 310–320. *J*, intensity ratio of ^{15}N hnRNP A2 266–341 to Fyn-SH3 showed decreased signal intensity at high concentrations of Fyn-SH3, consistent with induction of LLPS.

SH3. Therefore, Fyn-SH3 is not able to prevent hnRNP A2 LC aggregation in all conditions tested.

NMR experiments mixing hnRNP A2 LC subpeptides with Fyn-SH3 identify potential binding sites on Fyn-SH3

The purpose of our earlier two-dimensional NMR experiments was to characterize the structural details of the interaction between hnRNP A2 LC and Fyn-SH3. This proved difficult as hnRNP A2 LC phase-separated upon the addition of Fyn-SH3, sending the interacting proteins into viscous phase-separated droplets that are difficult to detect by solution NMR (12). To use NMR to identify the site of interac-

tion, we hypothesized that smaller pieces of hnRNP A2 LC will discourage LLPS but retain the ability to bind Fyn-SH3. We started with a subpeptide of hnRNP A2 containing residues 266–341, which contains the prion-like domain (residues 266–303; Fig. 4A). The prion-like domain in hnRNP A2 has been indicated in past studies to induce aggregation in neurodegenerative disease (15), and this domain contains the residues that are mutated in hnRNP A2-related degenerative diseases (Pro-298 and Asp-290). Furthermore, this subpeptide contains four of the nine total proline residues in the LC, which may act as binding sites for SH3 domains. As we had hoped, mixtures of Fyn-SH3 and hnRNP A2 266–341 in

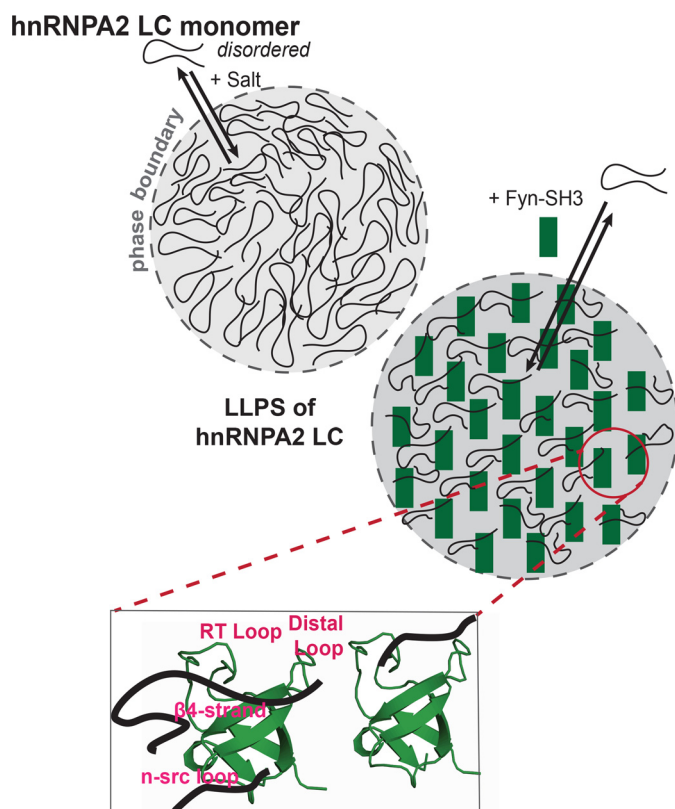


Figure 5. Fyn-SH3 may induce the phase separation of hnRNPA2 LC via contacts with the RT loop, β 4 strand, distal loop, and/or n-Src loop. Fyn-SH3 interacts with hnRNPA2 LC via multivalent/multisite contacts, introducing both a novel role for single folded domains in inducing disordered domain LLPS *in vitro* and suggesting a possible physiological role for Fyn-SH3 in Fyn function.

NMR buffer showed no phase separation at the concentrations tested.

We obtained NMR spectra at 1:1, 1:1.5, and 1:2 titrations of ^{15}N -labeled Fyn-SH3 to hnRNPA2 266–341 (20 μM Fyn-SH3) (Fig. 4B and Fig. S3A). As the concentration of the hnRNPA2 subpeptide was increased, we observed small but increasing chemical shift perturbations of Fyn-SH3 resonances (Fig. 4B and Fig. S3A), consistent with our microscopy experiments that suggest an interaction between Fyn-SH3 and hnRNPA2 LC. ^1H and ^{15}N chemical shift perturbations increased as a function of increasing concentration of the hnRNPA2 subpeptide (Fig. 4, C and D). These shifts are small, consistent with weak interactions often present in phase-separating protein partners (23). When the residues of Fyn-SH3 that experienced shifts are mapped on the structure of Fyn-SH3, they occur at surprising locations. We initially hypothesized that hnRNPA2 would interact with Fyn-SH3 through the n-Src loop, as shown for a proline-rich segment solved by NMR (20). However, the chemical shifts mainly occur in the RT loop, the β 4 strand, and the distal loop of Fyn-SH3 (Figs. 4E and 5). This SH3 surface overlaps with the binding surface region identified in multiple studies to bind to proline-rich motifs (24) and has been referred to as the “specificity zone.” The specificity zone is composed of the β 3 and β 4 strand, flanked by the far end of the n-Src loop and part of the RT loop (24) (Fig. 5). The most significant chemical shift perturbations occur in a part of this region, suggesting that

Fyn-SH3 interacts with hnRNPA2 through this specificity zone. Specifically, Thr-53 and Gly-54 on the β 4 strand and Leu-24 in the RT loop show the highest shifts (Fig. 4E). Unlike NMR experiments on Fyn-SH3 with the entire hnRNPA2 LC, these mixtures are stable and not prone to LLPS, as evidenced by intensity ratios around 1 (Fig. 4F). However, despite no visual evidence for phase separation, at 1:2, the intensity ratio decreases to ~ 0.7 (Fig. 4F), which may occur due to formation of higher-order assemblies.

We also performed the inverse experiment with ^{15}N hnRNPA2 266–341 and natural abundance Fyn-SH3 to attempt to identify Fyn-SH3-binding sites on hnRNPA2. We observed small chemical shift perturbations (Fig. 4 (G–I) and Fig. S3B) in hnRNPA2 266–341 across the whole subpeptide. In the region of 310–320, we observed a cluster of larger ^{15}N shifts, suggesting increased Fyn-SH3 binding with this region (Fig. 4I). Interestingly, when Fyn-SH3 was added at 5 molar eq to hnRNPA2 266–341, we observed slight turbidity in the NMR sample and corresponding signal loss, leaving about 60% of the 1:1 signal (Fig. 4J), suggesting that Fyn-SH3 can still induce phase separation of this small truncation of hnRNPA2.

In an attempt to probe the interaction of Fyn-SH3 with the remainder of hnRNPA2 LC, we generated a subpeptide encompassing hnRNPA2 190–303. However, in our standard conditions, this peptide immediately precipitated. Therefore, we performed NMR experiments at a lower pH (4.5), where hnRNPA2 LC is less assembly-prone. Here, the hnRNPA2 190–303 phase-separated upon the addition of equimolar Fyn-SH3, so we were unable to observe any significant chemical shift perturbations (Fig. S3, C–E). Hence, it appears that protein–protein interaction occurs, but LLPS precludes straightforward evaluation of the site-specific details of the interaction by NMR. This subpeptide does have more proline residues (7 total) than the 266–341 subpeptide; hence, this region may be a major contributor to Fyn-SH3 interaction with hnRNPA2.

Discussion

These NMR experiments identified hnRNPA2 LC interactions with the β 4 strand, RT loop, and distal loop of Fyn-SH3. Other groups have characterized similar interactions with the SH3 domain and other proline-rich proteins and refer to this surface region as the specificity zone (24). We saw significant chemical shift perturbations of the residues in the β 4 strand and the RT loop that are conserved across many SH3 domains (25), suggesting that these residues are important for SH3 function. Residues Asp-23 and Leu-24 in the RT loop of Fyn-SH3 showed large chemical shift perturbations in the presence of hnRNPA2 266–341. Chemical shift perturbations were observed in these same conserved residues of Noxa1-SH3 upon binding of Noxa1 proline-rich region (25). Another study claims that the binding of Fyn-SH3 to proline-rich proteins is mediated by weak interactions between the hydroxyl groups of the tyrosines in the n-Src loop region of SH3 and the backbone of the proline residues (26). Here, we see chemical shift perturbation at Asp-41 of the n-Src loop and the spatially proximate Tyr-14, suggesting that there may be a second interface for hnRNPA2 LC binding. Additionally, the negatively charged binding surfaces of Fyn-SH3 have been implicated in other

interactions between proline-rich proteins and Fyn-SH3 (27). hnRNP A2 is positively charged, with a pI of 9.30, so electrostatic interactions may contribute to the interaction and phase separation of the mixture. However, the interaction is not due to weak electrostatics contact artifacts from low-conductivity buffers as we still observed the formation of a large, NMR-invisible species when hnRNP A2 LC with a solubility tag was mixed with Fyn-SH3 in the presence of salt. With a truncated hnRNP A2 LC(266–341), we were able to observe some chemical shift perturbations upon Fyn-SH3 binding. The largest shifts were localized to residues 314–325, a region that contains a proline-tyrosine nuclear localization signal (PY-NLS) (residues 318–324) that binds the importin transportin-1 (karyopherin β -2). Intriguingly, transportin-1 binding to the PY-NLS of FUS, a related hnRNP with a prion-like domain, disrupts FUS phase separation (28–30). Therefore, PY-NLSs may serve as prominent binding sites regulating phase separation. However, our data do not definitively identify the PY-NLS as the highest affinity Fyn-SH3-binding site in hnRNP A2 LC because the addition of Fyn-SH3 to both the intact LC and an N-terminal fragment (residues 190–303) resulted in phase separation at lower concentrations than with the 266–341 truncation, possibly due to higher affinity binding and precluding determination of chemical shift perturbations.

Understanding how Fyn-SH3 binds to target proteins and identifying the binding interfaces between Fyn-SH3 and those targets, like hnRNP A2, is important for the potential development of therapeutics for degenerative diseases. Past studies have shown that the Nck-SH3 domains induce phase separation via multivalent interactions (31–33). Phase separation of Nck and N-WASP depends on the number of SH3 domains; one SH3 domain is not sufficient to induce phase separation, and Nck normally contains three SH3 domains (33). In contrast, our study shows that the single Fyn-SH3 domain is sufficient to induce phase separation of hnRNP A2 LC. The Fyn-SH3 domain itself may be a multivalent binding platform for hnRNP A2 LC; our NMR data indicate multiple sites on Fyn-SH3 that can bind to hnRNP A2 LC. Interestingly, the presence of multiple interaction sites implies a potential mechanism for how this single, monomeric SH3 domain induces phase separation of hnRNP A2 LC. This model has multiple hnRNP A2 LC molecules binding to different sites on Fyn-SH3 simultaneously, enhancing hnRNP A2 LC intermolecular interactions and initiating network-spanning contacts. Alternatively, multiple hnRNP A2 LC molecules could also bind to a single site/region on Fyn-SH3 (e.g. a site that can accommodate several proline residues simultaneously).

The induction of LLPS of hnRNP A2 LC is not likely to be the physiological role of Fyn-SH3, as hnRNP A2 would already be phase-separated within an RNA granule when it then interacts with membrane-tethered Fyn-kinase present at the oligodendroglial site of local translation. We suggest that multivalent Fyn-SH3–hnRNP A2 contacts aid Fyn incorporation into hnRNP A2 granules to spatially control the interaction of the kinase domain of Fyn and hnRNP A2, leading to hnRNP A2 phosphorylation and granule disassembly at sites where local translation is needed. Partitioning of Fyn into hnRNP A2 granules may also speed the phosphorylation reaction due to increased

local concentrations of hnRNP A2, Fyn-kinase, and ATP (6). Tight spatial and temporal control of the dissociation of mRNA transport granules is critical to ensure that the mRNAs are translated only when and where the protein is needed. As phosphorylation also reduces phase separation of another granule protein, FUS (34), it is possible that other kinases co-phase-separate with their target granule proteins and dissociate the phase-separated granule from inside the phase-separated state. More work is needed to understand the molecular details underlying granule dissociation and whether incorporation of kinases into the granule is a common mechanism that can be targeted to prevent aggregation of mutant protein from the phase-separated state.

Experimental procedures

Constructs

The following constructs and purification strategies were used for protein expression in BL21 Star (DE3) *Escherichia coli* (Life Technologies, Inc.): Fyn-SH3, soluble His-tag purification (Addgene ID 118823); Fyn-SH3 S25C, soluble His-tag purification (Addgene ID 118824); hnRNP A2 LC (residues 190–341), insoluble His-tag purification (Addgene ID 98657); hnRNP A2 LC (residues 190–341) D290V, insoluble His-tag purification (Addgene ID 98658); hnRNP A2 LC (residues 190–341) P298L, insoluble His-tag purification (Addgene ID 104465); hnRNP A2 266–341, insoluble His-tag purification (Addgene ID 118821); hnRNP A2 190–303, insoluble His-tag purification (Addgene ID 118822). Fyn-SH3 was a gift from David Libich.

Bacterial culture and isotope labeling

Proteins were expressed in either Luria broth or M9 minimal medium containing ^{15}N ammonium chloride as the sole nitrogen source for ^{15}N labeling. BL21 Star DE3 *E. coli* cells were grown at 37 °C with 50 mg/liter kanamycin or 100 mg/liter ampicillin as appropriate until the A_{600} reached 0.6–1, and then the cultures were induced with 1 mM isopropyl- β -D-thiogalactoside at 37 °C for 4 h. Cells were collected by centrifugation. The cell pellet was resuspended in 20 mM sodium phosphate (NaP_i), pH 7.4, 300 mM NaCl, 10 mM imidazole for hnRNP A2 proteins and 50 mM Tris, pH 8.0, 500 mM NaCl, 10 mM imidazole for Fyn-SH3 protein. Once cleared by resuspension, cells were lysed using an Emulsiflex C3 homogenizer (Avestin). The cell lysates were cleared by centrifugation at $20,000 \times g$ for 60 min at 4 °C.

Protein purification

hnRNP A2—hnRNP A2 constructs were purified as described (12). Briefly, after expression and cell lysis, inclusion bodies were resuspended in 8 M urea, 20 mM NaP_i , pH 7.4, 300 mM NaCl, 10 mM imidazole. After centrifugation at $20,000 \times g$ for 1 h, the supernatant was collected, filtered, and loaded onto a HisTrap HP 5-ml column. Protein was eluted using a gradient from 10 to 300 mM imidazole over 5 column volumes. Pooled fractions containing the desired protein were buffer-exchanged into 8 M urea, pH 5.5, MES and concentrated to 1 ml. Urea was diluted out by adding 20 ml of 20 mM MES, pH 5.5 (pH-adjusted with BisTris). The protein was incubated with TEV protease

overnight at room temperature. To resolubilize precipitated protein, 8 M urea, 20 mM NaP_i, 300 mM NaCl, 10 mM imidazole was added to the protein. Protein was filtered and loaded onto a HisTrap HP 5-ml column to remove the TEV protease, cleaved His-tag, and uncleaved protein. Flow-through fractions containing the purified product were concentrated and buffer-exchanged into 8 M urea, pH 5.5, MES and flash-frozen.

Fyn-SH3—As Fyn-SH3 is soluble, the cleared lysate was filtered using a 0.2- μ m filter and loaded onto a HisTrap HP 5-ml column. Protein was eluted using a gradient from 10 to 300 mM imidazole over 5 column volumes. The fractions containing Fyn-SH3 were pooled and incubated with TEV protease overnight at room temperature. To remove the His-tag, the protein was loaded onto a Superdex 75 column equilibrated in 50 mM Tris, pH 8.0, 150 mM NaCl, 2 mM EDTA. The fractions containing the purified Fyn-SH3 protein were concentrated and buffer-exchanged into pH 5.5 MES and flash-frozen for storage. For labeling experiments, Fyn-SH3 S25C was expressed and purified as described above, with the addition of 1 mM DTT to all buffers.

Alexa Fluor labeling

Fyn-SH3 S25C was labeled using Alexa FluorTM 488 C5 maleimide (Life Technologies), which reacts with free thiol groups. After Fyn-SH3 S25C was purified, 2 ml ZebaTM spin desalting columns (Thermo Fisher Scientific) were used to remove the DTT and buffer-exchange the protein into pH 7.5, 50 mM Tris buffer. After desalting, the protein was incubated with excess Alexa Fluor C5 maleimide at room temperature for 2 h (covered in aluminum foil), according to the manufacturer's procedures. This reaction mixture was then placed into an equilibrated desalting column to remove excess label. The protein was buffer-exchanged into 20 mM MES, pH 5.5 (pH-adjusted with BisTris) and flash-frozen. The concentration of the protein was quantified by Nanodrop 2000c using the Alexa-488 setting, which is programmed to account for Alexa FluorTM 488 labeling.

Solution NMR experiments

NMR titration experiments were acquired using a Bruker Avance III HD NMR spectrometer operating at 850 MHz, ¹H Larmor frequency equipped with HCN TCI z-gradient cryoprobe. The temperature was set at 25 °C. Experimental sweep widths, acquisition times, and the number of transients were optimized for the necessary resolution, experiment time, and signal/noise ratio.

Two-dimensional NMR titration experiments

hnRNP2 LC was diluted to the appropriate concentration for the experiment from 8 M urea, 20 mM MES, pH 5.5 (pH-adjusted with BisTris), ensuring that the urea concentration was consistently 150 mM. Fyn-SH3 was diluted to the appropriate concentration from 20 mM MES, pH 5.5. Each sample contained 10% D₂O. 1:0 samples (regardless of ¹⁵N-labeled species) contained 20 μ M protein in the absence of unlabeled titrant protein; protein concentration ratios for the titrant protein or peptide are calculated from that concentration (e.g. 1:2 is 20 μ M

¹⁵N-labeled protein plus 40 μ M unlabeled titrant protein). This applies to all data except for Fig. 1A, as labeled.

Chemical shift perturbations were calculated by subtracting the chemical shifts of the reference peaks (1:0 titrations) from the chemical shifts acquired in the titration experiments. Intensity ratios were calculated from the height of each peak, and the uncertainty was estimated from the signal/noise ratio of each spectrum. Data were plotted using Prism (GraphPad Software, Inc.).

hnRNP2 NMR assignments

hnRNP2 LC and 266–341 assignments are available from the Biological Magnetic Resonance Data Bank (BMRB) (LC BMRB entry 27123 (12), 266–341 BMRB entry 27649). Assignments for hnRNP2 266–341 were performed on a sample of uniformly ¹³C/¹⁵N-labeled hnRNP2 266–341 at 125 μ M in 20 mM MES, pH 5.5, 150 mM urea, 10% ²H₂O, 25 °C. Briefly, CBCA(CO)NH, HNCACB, HNCO, HN(CA)CO experiments with sweep widths of 10 ppm (CBCA(CO)NH only) or 13 ppm in ¹H (center 4.7), 17 ppm in ¹⁵N (center 115.5), 6 ppm (center 175.5) in ¹³C for CO experiments, 42 ppm (center 46.7) in ¹³C for CA/CB experiments were performed using standard Bruker Topspin 3.2 experiments with default parameter sets. Experiments comprised 72–130, 218, 72–94, 86, and 3072–4096 total points in the indirect ¹⁵N, indirect ¹³Ca, indirect ¹³Ca/C β , indirect ¹³CO, and direct ¹H dimensions, respectively. Fyn-SH3 assignments were a gift of David Libich.

Fluorescence and DIC microscopy

DIC images and fluorescence microscopy of Fyn-SH3, Fyn-SH3 Alexa Fluor, and hnRNP2 LC WT, P298L, and D290V proteins were collected at pH 5.5, 20 mM MES buffer conditions. NaCl was omitted unless specified. Experimental samples were prepared by diluting proteins into experimental conditions with a final volume of 50 μ l. Differential interference contrast on an Axiovert 200M microscope (Zeiss) was used to observe hnRNP2 LC droplets and aggregates. Fluorescence microscopy on an Axiovert 200M microscope (Zeiss) was used to observe Alexa Fluor-labeled Fyn-SH3 incorporation in hnRNP2 LC droplets. Samples were spotted on a coverslip for imaging. Images were processed with ImageJ (National Institutes of Health).

A600 turbidity experiments

Turbidity experiments were performed in 96-well clear plates (Costar) with 65- μ l samples sealed with clear optical adhesive film (MicroAmp, Thermo Fisher Scientific). Cytation 3 Cell Imaging Multi-Mode Reader (BioTek) was used to record the turbidity by measuring the optical density at 600 nm at 5-min time intervals for up to 12 h. The samples were premixed for 5 s before the start of the recordings, and readings were made from the bottom of the plate. Each sample was placed in three wells to acquire average and S.D. Sample turbidity values were subtracted from the buffer control value.

Turbidity experiments of hnRNP2 LC and Fyn-SH3 were conducted by diluting hnRNP2 LC WT to 20 μ M (maintaining a final concentration of 150 mM urea). Both proteins were diluted into 20 mM MES, pH 5.5. The amount of Fyn-SH3 con-

Fyn-SH3 induces hnRNP A2 LC phase separation

centrations was added in appropriate ratios to hnRNP A2 LC concentrations. Statistical analysis was performed with Microsoft Excel 360, and data were graphed using Prism (GraphPad Software).

Aggregation by microscopy assay

To study the effects of Fyn-SH3 on the progression of hnRNP A2 LC WT aggregate formation, Fyn-SH3 was mixed with either hnRNP A2 LC WT, D290V, or P298L. Each protein was diluted into 50- μ L samples at 20 mM MES, pH 5.5. NaCl was omitted unless otherwise indicated. hnRNP A2 LC variants were diluted to 20 μ M, which diluted the 8 M urea from the storage solution to a concentration of 150 mM residual urea for the final experimental conditions. Fyn-SH3 was diluted to 20 μ M concentrations as well and placed into each tube as appropriate. Each sample contained either a 1:0 ratio of the hnRNP A2 LC variant to Fyn-SH3 or a 1:1 ratio of the hnRNP A2 LC variant to Fyn-SH3. 20 μ L of each sample was pipetted to a coverslip and observed using differential interference contrast on an Axiovert 200M microscope (Zeiss). This was done immediately after the sample was prepared. Two replicates were prepared, one for observation at 0 h and the other for observation at 3 h. Images were processed and analyzed using ImageJ (National Institutes of Health).

Author contributions—J. A. and V. H. R. investigation; J. A. and V. H. R. writing-original draft; V. H. R. and N. L. F. conceptualization; V. H. R. and N. L. F. methodology; N. L. F. project administration; V. H. R. and N. L. F. writing-review and editing; N. L. F. resources; N. L. F. supervision; N. L. F. funding acquisition.

Acknowledgments—We thank David Libich for the gift of the plasmid encoding Fyn-SH3 and corresponding Fyn-SH3 NMR assignments. We thank Rute Silva for creation of some of the hnRNP A2 LC truncation constructs.

References

- Brangwynne, C. P., Eckmann, C. R., Courson, D. S., Rybarska, A., Hoeghe, C., Gharakhani, J., Jülicher, F., and Hyman, A. A. (2009) Germline P granules are liquid droplets that localize by controlled dissolution/condensation. *Science* **324**, 1729–1732 [CrossRef Medline](#)
- Aguilera-Gomez, A., and Rabouille, C. (2017) Membrane-bound organelles versus membrane-less compartments and their control of anabolic pathways in *Drosophila*. *Dev. Biol.* **428**, 310–317 [CrossRef Medline](#)
- Larson, A. G., Elnatan, D., Keenen, M. M., Trnka, M. J., Johnston, J. B., Burlingame, A. L., Agard, D. A., Redding, S., and Narlikar, G. J. (2017) Liquid droplet formation by HP1 α suggests a role for phase separation in heterochromatin. *Nature* **547**, 236–240 [CrossRef Medline](#)
- Sheu-Gruttadauria, J., and MacRae, I. J. (2018) Phase transitions in the assembly and function of human miRISC. *Cell* **173**, 946–957.e16 [CrossRef Medline](#)
- Nott, T. J., Craggs, T. D., and Baldwin, A. J. (2016) Membraneless organelles can melt nucleic acid duplexes and act as biomolecular filters. *Nat. Chem.* **8**, 569–575 [CrossRef Medline](#)
- Shin, Y., and Brangwynne, C. P. (2017) Liquid phase condensation in cell physiology and disease. *Science* **357**, eaaf4382 [CrossRef Medline](#)
- Guo, L., and Shorter, J. (2015) It's raining liquids: RNA tunes viscoelasticity and dynamics of membraneless organelles. *Mol. Cell* **60**, 189–192 [CrossRef Medline](#)
- Shin, Y., Berry, J., Pannucci, N., Haataja, M. P., Toettcher, J. E., and Brangwynne, C. P. (2017) Spatiotemporal control of intracellular phase transitions using light-activated optoDroplets. *Cell* **168**, 159–171.e14 [CrossRef Medline](#)
- Boggon, T. J., and Eck, M. J. (2004) Structure and regulation of Src family kinases. *Oncogene* **23**, 7918–7927 [CrossRef Medline](#)
- Kapeli, K., Martinez, F. J., and Yeo, G. W. (2017) Genetic mutations in RNA-binding proteins and their roles in ALS. *Hum. Genet.* **136**, 1193–1214 [CrossRef Medline](#)
- Shan, J., Moran-Jones, K., Munro, T. P., Kidd, G. J., Winzor, D. J., Hoek, K. S., and Smith, R. (2000) Binding of an RNA trafficking response element to heterogeneous nuclear ribonucleoproteins A1 and A2. *J. Biol. Chem.* **275**, 38286–38295 [CrossRef Medline](#)
- Ryan, V. H., Dignon, G. L., Zerze, G. H., Chabata, C. V., Silva, R., Conicella, A. E., Amaya, J., Burke, K. A., Mittal, J., and Fawzi, N. L. (2018) Mechanistic view of hnRNP A2 low-complexity domain structure, interactions, and phase separation altered by mutation and arginine methylation. *Mol. Cell* **69**, 465–479.e7 [CrossRef Medline](#)
- Prusiner, S. B. (2013) Biology and genetics of prions causing neurodegeneration. *Annu. Rev. Genet.* **47**, 601–623 [CrossRef Medline](#)
- King, O. D., Gitler, A. D., and Shorter, J. (2012) The tip of the iceberg: RNA-binding proteins with prion-like domains in neurodegenerative disease. *Brain Res.* **1462**, 61–80 [CrossRef Medline](#)
- Kim, H. J., Kim, N. C., Wang, Y. D., Scarborough, E. A., Moore, J., Diaz, Z., MacLea, K. S., Freibaum, B., Li, S., Molliex, A., Kanagaraj, A. P., Carter, R., Boylan, K. B., Wojtas, A. M., Rademakers, R., et al. (2013) Mutations in prion-like domains in hnRNP A2B1 and hnRNP A1 cause multisystem proteinopathy and ALS. *Nature* **495**, 467–473 [CrossRef Medline](#)
- White, R., and Krämer-Albers, E. M. (2014) Axon-glia interaction and membrane traffic in myelin formation. *Front. Cell Neurosci.* **7**, 284 [Medline](#)
- White, R., Gonsior, C., Krämer-Albers, E. M., Stöhr, N., Hüttelmaier, S., and Trotter, J. (2008) Activation of oligodendroglial Fyn kinase enhances translation of mRNAs transported in hnRNP A2-dependent RNA granules. *J. Cell Biol.* **181**, 579–586 [CrossRef Medline](#)
- Zarrinpar, A., Bhattacharyya, R. P., and Lim, W. A. (2003) The structure and function of proline recognition domains. *Sci. STKE* **2003**, RE8 [Medline](#)
- Krämer-Albers, E. M., and White, R. (2011) From axon-glia signalling to myelination: the integrating role of oligodendroglial Fyn kinase. *Cell Mol. Life Sci.* **68**, 2003–2012 [CrossRef Medline](#)
- Renzoni, D. A., Pugh, D. J., Siligardi, G., Das, P., Morton, C. J., Rossi, C., Waterfield, M. D., Campbell, I. D., and Ladbury, J. E. (1996) Structural and thermodynamic characterization of the interaction of the SH3 domain from Fyn with the proline-rich binding site on the p85 subunit of PI3-kinase. *Biochemistry* **35**, 15646–15653 [CrossRef Medline](#)
- Conicella, A. E., Zerze, G. H., Mittal, J., and Fawzi, N. L. (2016) ALS Mutations disrupt phase separation mediated by α -helical structure in the TDP-43 low-complexity C-terminal domain. *Structure* **24**, 1537–1549 [CrossRef Medline](#)
- Wegmann, S., Eftekharzadeh, B., Tepper, K., Zoltowska, K. M., Bennett, R. E., Dujardin, S., Laskowski, P. R., MacKenzie, D., Kamath, T., Commins, C., Vanderburg, C., Roe, A. D., Fan, Z., Molliex, A. M., Hernandez-Vega, A., et al. (2018) Tau protein liquid-liquid phase separation can initiate tau aggregation. *EMBO J.* **37**, e98049 [CrossRef Medline](#)
- Wang, J., Choi, J. M., Holehouse, A. S., Lee, H. O., Zhang, X., Jahnel, M., Maharana, S., Lemaître, R., Pozniakovsky, A., Drechsel, D., Poser, I., Pappu, R. V., Alberti, S., and Hyman, A. A. (2018) A Molecular grammar governing the driving forces for phase separation of prion-like RNA binding proteins. *Cell* **174**, 688–699.e16 [CrossRef Medline](#)
- Saksela, K., and Permi, P. (2012) SH3 domain ligand binding: what's the consensus and where's the specificity? *FEBS Lett.* **586**, 2609–2614 [CrossRef Medline](#)
- Shrestha, P., Yun, J. H., Ko, Y. J., Kim, M., Bae, Y. S., and Lee, W. (2017) C-terminal tail of NADPH oxidase organizer 1 (Noxo1) mediates interaction with NADPH oxidase activator (Noxa1) in the NOX1 complex. *Biochem. Biophys. Res. Commun.* **490**, 594–600 [CrossRef Medline](#)
- Kang, H., Freund, C., Duke-Cohan, J. S., Musacchio, A., Wagner, G., and Rudd, C. E. (2000) SH3 domain recognition of a proline-independent tyrosine-based RKxxYxxY motif in immune cell adaptor SKAP55. *EMBO J.* **19**, 2889–2899 [CrossRef Medline](#)

27. Polverini, E., Rangaraj, G., Libich, D. S., Boggs, J. M., and Harauz, G. (2008) Binding of the proline-rich segment of myelin basic protein to SH3 domains: spectroscopic, microarray, and modeling studies of ligand conformation and effects of posttranslational modifications. *Biochemistry* **47**, 267–282 [CrossRef Medline](#)
28. Yoshizawa, T., Ali, R., Jiou, J., Fung, H. Y. J., Burke, K. A., Kim, S. J., Lin, Y., Peeples, W. B., Saltzberg, D., Soniat, M., Baumhardt, J. M., Oldenbourg, R., Sali, A., Fawzi, N. L., Rosen, M. K., and Chook, Y. M. (2018) Nuclear import receptor inhibits phase separation of FUS through binding to multiple sites. *Cell* **173**, 693–705.e22 [CrossRef Medline](#)
29. Hofweber, M., Hutten, S., Bourgeois, B., Spreitzer, E., Niedner-Boblentz, A., Schifferer, M., Ruepp, M. D., Simons, M., Niessing, D., Madl, T., and Dormann, D. (2018) Phase separation of FUS is suppressed by its nuclear import receptor and arginine methylation. *Cell* **173**, 706–719.e13 [CrossRef Medline](#)
30. Guo, L., Kim, H. J., Wang, H., Monaghan, J., Freyermuth, F., Sung, J. C., O'Donovan, K., Fare, C. M., Diaz, Z., Singh, N., Zhang, Z. C., Coughlin, M., Sweeny, E. A., DeSantis, M. E., Jackrel, M. E., *et al.* (2018) Nuclear-import receptors reverse aberrant phase transitions of RNA-binding proteins with prion-like domains. *Cell* **173**, 677–692.e20 [CrossRef Medline](#)
31. Banjade, S., Wu, Q., Mittal, A., Peeples, W. B., Pappu, R. V., and Rosen, M. K. (2015) Conserved interdomain linker promotes phase separation of the multivalent adaptor protein Nck. *Proc. Natl. Acad. Sci. U.S.A.* **112**, E6426–E6435 [CrossRef Medline](#)
32. Harmon, T. S., Holehouse, A. S., Rosen, M. K., and Pappu, R. V. (2017) Intrinsically disordered linkers determine the interplay between phase separation and gelation in multivalent proteins. *Elife* **6**, e30294 [CrossRef Medline](#)
33. Li, P., Banjade, S., Cheng, H. C., Kim, S., Chen, B., Guo, L., Llaguno, M., Hollingsworth, J. V., King, D. S., Banani, S. F., Russo, P. S., Jiang, Q. X., Nixon, B. T., and Rosen, M. K. (2012) Phase transitions in the assembly of multivalent signalling proteins. *Nature* **483**, 336–340 [CrossRef Medline](#)
34. Monahan, Z., Ryan, V. H., Janke, A. M., Burke, K. A., Rhoads, S. N., Zerze, G. H., O'Meally, R., Dignon, G. L., Conicella, A. E., Zheng, W., Best, R. B., Cole, R. N., Mittal, J., Shewmaker, F., and Fawzi, N. L. (2017) Phosphorylation of the FUS low-complexity domain disrupts phase separation, aggregation, and toxicity. *EMBO J.* **36**, 2951–2967 [CrossRef Medline](#)

The SH3 domain of Fyn kinase interacts with and induces liquid–liquid phase separation of the low-complexity domain of hnRNPA2

Joshua Amaya, Veronica H. Ryan and Nicolas L. Fawzi

J. Biol. Chem. 2018, 293:19522–19531.

doi: 10.1074/jbc.RA118.005120 originally published online November 5, 2018

Access the most updated version of this article at doi: [10.1074/jbc.RA118.005120](https://doi.org/10.1074/jbc.RA118.005120)

Alerts:

- [When this article is cited](#)
- [When a correction for this article is posted](#)

[Click here](#) to choose from all of JBC's e-mail alerts

This article cites 34 references, 6 of which can be accessed free at <http://www.jbc.org/content/293/51/19522.full.html#ref-list-1>